Geophysical Research Letters

RESEARCH LETTER
10.1029/2020GL091299

Diurnal Ocean Surface Warming Drives Convective Turbulence and Clouds in the Atmosphere

Simon P. de Szoeke[1], Tobias Marke[2], and W. Alan Brewer[3]

[1]Oregon State University, Corvallis, OR, USA, [2]CIRES, University of Colorado Boulder, NOAA Chemical Sciences Laboratory, Boulder, CO, USA, [3]NOAA Chemical Sciences Laboratory, Boulder, CO, USA

Key Points:

- A vast area of the ocean surface warms in the afternoon under calm winds, enhancing surface buoyancy flux to the atmosphere
- Diurnally enhanced buoyancy flux from the ocean generates a diurnal convective turbulent mixed layer in the atmosphere
- Enhanced afternoon marine atmospheric turbulence forms clouds by mixing moisture to its condensation level

Supporting Information:

- Supporting Information S1

Correspondence to:

S. P. de Szoeke,
simon.deszoeke@oregonstate.edu

Citation:

de Szoeke, S. P., Marke, T., & Brewer, W. A. (2021). Diurnal ocean surface warming drives convective turbulence and clouds in the atmosphere. *Geophysical Research Letters*, *48*, e2020GL091299. https://doi.org/10.1029/2020GL091299

Received 15 OCT 2020
Accepted 17 DEC 2020

Abstract Sunlight warms sea surface temperature (SST) under calm winds, increasing atmospheric surface buoyancy flux, turbulence, and mixed layer (ML) depth in the afternoon. The diurnal range of SST exceeded 1°C for 24% of days in the central tropical Indian Ocean during the Dynamics of the Madden Julian Oscillation experiment in October-December 2011. Doppler lidar shows enhancement of the strength and height of convective turbulence in the atmospheric ML over warm SST in the afternoon. The turbulent kinetic energy (TKE) dissipation rate of the marine atmospheric ML scales with surface buoyancy flux like previous measurements of convective MLs. The time of enhanced ML TKE dissipation rate is out of phase with the buoyancy flux generated by nocturnal net radiative cooling of the atmosphere. Diurnal atmospheric convective turbulence over the ocean mixes moisture from the ocean to the lifting condensation level and forms afternoon clouds.

Plain Language Summary Howard's (1803) original description of cumulus clouds includes convection (overturning by heating from below) in the heat of the afternoon. When wind is weak, sunlight warms vast and variable areas of the ocean (some 5% of the tropical oceans and 2% of Earth's surface) by more than 1°C in the afternoon. Convection and turbulence form over the warmed ocean like over land. We show the afternoon strengthening and deepening of the turbulence. The afternoon convection raises water vapor from the ocean surface, moistens the atmosphere, and forms clouds.

1. Introduction

Diurnal warming of the ocean surface is expected to generate turbulence, but measurements of the diurnal vertical profile of marine atmospheric turbulence have never been documented. The afternoon warming of the ocean is much weaker than that of land because the ocean mixes and stores heating over meters to tens of meters. Temperature-stratified diurnal warm layers (DWLs), resulting from strong solar absorption and weak winds (Fairall et al., 1996, Price et al., 1986, reviewed in Kawai & Wada 2007), increase the sea surface temperature (SST) in the afternoon. Clear skies result in more solar absorption. Weak winds result in weak turbulent fluxes and ocean mixing, with DWLs possible for winds under 7.6 m s^{-1} (Thompson et al., 2019).

Over tropical oceans, strong nocturnal atmospheric radiative cooling generates strongest precipitation in the early morning. A secondary peak in the early afternoon is due to diurnal warming of SST (Bellenger et al., 2010; Chen & Houze 1997; Eastman & Warren 2014; Gray & Jacobson 1977; Randall et al., 1991; Sui et al., 1997). The lack of diurnal cycles in SST and boundary layer convection in general circulation models causes errors in the phase and amplitude of precipitation (Dai & Trenberth 2004; Tian et al., 2004).

In the tropics, diurnal SST range (dSST) is strong under weak winds in areas of convergence and between storms. These conditions are most common in the eastern tropical Pacific intertropical convergence zone, in the convergence of Western Pacific summer monsoon westerlies and easterly trade winds, and during phases of suppressed precipitation of tropical intraseasonal variability (Clayson & Weitlich 2007; C. L. Gentemann & Akella 2018) such as the Madden Julian Oscillation (MJO).

Diurnal SST observed in the Mirai Indian Ocean cruise for Study of the MJO-convection Onset (MISMO) and Dynamics of the Madden Julian Oscillation (DYNAMO) experiments locally moistened and warmed the atmospheric boundary layer, destabilized the atmosphere for precipitating convection (Bellenger et al., 2010; Ruppert & Johnson 2015), and increased integrated atmospheric water vapor (Yasunaga et al., 2008). Unsaturated convective boundary layer circulations have been observed to be responsible for fluxes of heat and

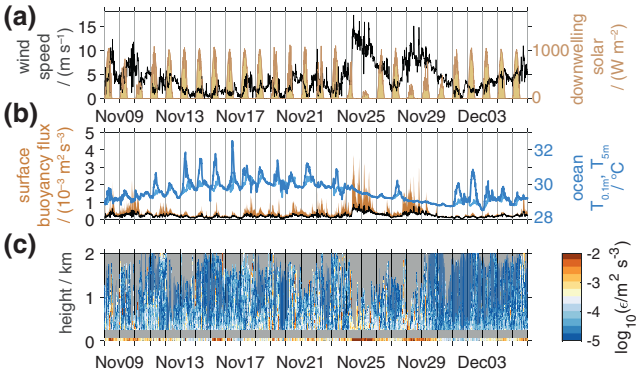

Figure 1. Time series of surface flux variables and turbulence profiles observed in Dynamics of the Madden Julian Oscillation (DYNAMO) leg 3 (Nov 8–Dec 6). (a) Current-relative wind speed (left, black) and downwelling solar radiation (right, yellow filled). (b) Surface buoyancy flux (left; total orange, black contribution from water vapor flux) and ocean temperature (right, blue) at 0.1 m and 5 m (light blue) depth. (c) Time-height series of turbulent kinetic energy (TKE) dissipation rate ϵ from Doppler lidar above 250 m. The shaded band at the surface is ϵ from the sonic anemometer at 20 m.

moisture to the free troposphere when clouds were suppressed (LeMone & Pennell 1976). Cloud resolving models show an afternoon increase in shallow convective clouds over the warm SST anomalies (Ruppert & Johnson 2016).

Here we document the diurnal response of turbulence that connects dSST to convective clouds. Turbulence over marine convective atmospheric mixed layers (MLs) has been observed previously by aircraft (Fairall et al., 1980; Frisch & Ochs 1975; Lenschow 1970). Ship-based remote sensing allows us to profile the turbulence throughout the diurnal cycle. Intensification and deepening of the turbulent atmospheric ML were observed by Doppler lidar over dSST anomalies in the central Indian Ocean in late 2011 during the Dynamics of the Madden Julian Oscillation (DYNAMO) experiment (Section 2). The ML turbulence is shown to scale with the buoyancy flux like previously observed convective MLs, including diurnal mixing over land (Section 3). Section 4 shows the connection of the turbulent ML to the clouds and summarizes its effect on atmospheric moist convective clouds over the ocean.

2. DYNAMO Observations

2.1. The Diurnal Warm Layer of SST in the Indian Ocean

The DYNAMO experiment in November-December 2011 sampled two suppressed and active phases of precipitating convective clouds related intraseasonal atmospheric variability (Madden & Julian 1971). DYNAMO days frequently had strong dSST. Median dSST was 0.58°C. The dSST was greater than 1°C for 19 (24%) of the 77 days, and greater than 1.5°C for seven of the days. Maximum dSST was 2.8°C. Diurnal warm layers did not form during two convective westerly wind bursts in late November (Figure 1b; Moum et al., 2014), but they formed on the days before, between, and after the wind bursts. The vertical structure of ocean DWLs was observed in DYNAMO from a ship (Hughes et al., 2020; Moulin et al., 2017), and by ocean gliders penetrating the surface (Matthews et al., 2014).

We focus on November 13–16, four consecutive days with dSST > 1.8°C (Figures 1b and 2b). These days were in the phase of suppressed intraseasonal precipitation (de Szoeke et al., 2015; Moum et al., 2014). At this time, weak winds reduced mechanical generation of turbulence in the atmosphere and the ocean and permitted stratification and warm SST anomalies to form in the ocean. SST warmed quickly during midday solar heating November 13–15 and cooled gradually at night (Figure 2d). On November 16, SST increased only modestly during mid-day and then quickly increased 2°C after 16 local time (LT). Quick cooling events related to 3–4.5 m s^{-1} gusts enhance the cooling during the afternoons of November 14 and 15.

2.2. Wind and Buoyancy Flux

Figures 1a and 1b shows the diurnal cycles of wind, solar radiation, ocean temperature at 0.1 and 5 m depth, and buoyancy flux for two month-long legs of the DYNAMO experiment (de Szoeke et al. 2015). Buoyancy flux at the surface depends on the temperature and water vapor flux,

$$B(0) = \frac{g}{T_v}\overline{w'T_v'} = \frac{g}{T_v}\left[\overline{w'T'}(1+\beta q) + \overline{w'q'}\beta T\right] = \frac{g}{\rho T_v}\left[\frac{H_s}{c_p}(1+\beta q) + \frac{H_l}{L_v}\beta T\right],$$

where T_v is the virtual temperature $T_v = p/R_d\rho = T\alpha$, q is the specific humidity, $\beta = R_v/R_d - 1 \approx 0.608$, and H_s, H_l are the sensible and latent surface turbulent heat fluxes. Over the warm tropical Indian Ocean, the thermal expansion of air and the lower density water vapor both contribute comparably to the buoyancy flux. Temperature and water vapor flux are products of wind speed and the sea-air surface difference of temperature and humidity, respectively. Surface buoyancy flux $B(0)$ observed in DYNAMO leg 3 (Nov 8–Dec 6, Figure 1b)

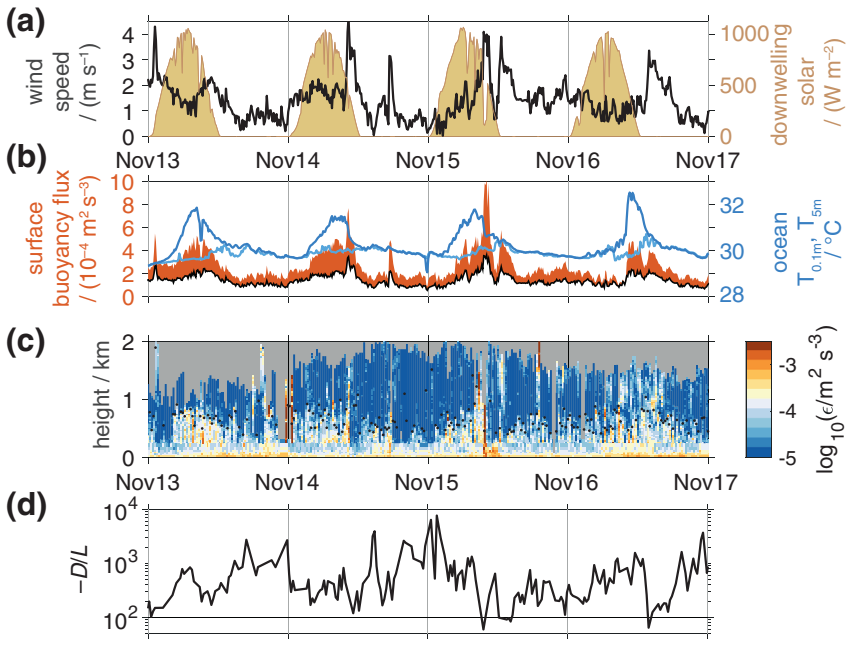

Figure 2. As for Figure 1 but for Nov 13–17, the 4-day period of sea surface temperature (SST) diurnal cycles. Black dots in panel c are diagnosed mixed layer depth D. TKE dissipation rate below 250 m is estimated by Doppler lidar azimuthal scans. (d) Ratio $-D/L$ of mixed layer depth to negative Monin-Obukhov length and the convective criterion $-D/L>10^2$.

is positive and lognormally distributed, with median$[B(0)] = 3.7 \times 10^{-4}$ and mean$[B(0)] = 4.8 \times 10^{-4}$. The friction velocity $u_* = \sqrt{|\tau| / \rho} \approx 0.04 U_{10\mathrm{rel}} = 0.1$ m s^{-1} for a weak wind of 2–3 m s^{-1} (typical for Nov 13–17, the time domain Figure 2a).

Wind speed dominates daily to intraseasonal variability of the latent and sensible turbulent surface fluxes in DYNAMO (de Szoeke et al. 2015). Average buoyancy flux is weak (3×10^{-4} m^2 s^{-3}) for wind below 3 m s^{-1} (Figure 1b). Mean wind from 6 to 14 LT is less than 2.6 m s^{-1} on each of the 7 days with dSST > 1.5°C (Section 2a). The buoyancy flux is weaker on these days, yet the diurnal cycle of buoyancy flux is coherent, with maximum daylight buoyancy flux (6×10^{-4} m^2 s^{-3}) 2.7 times greater than the predawn (0–6 h local) mean buoyancy flux.

For November 13–17, the buoyancy flux is strongly correlated to the SST anomalies (Figure 2b). The correlation coefficient R(SST, B) = 0.64 for Nov 13–17, and increases to R = 0.75 when computed for wind less than 3 m s^{-1}.

2.3. Turbulence Dissipation Rate Profiles

The diurnal enhancement of buoyancy flux generates turbulent convection in the subcloud boundary layer. The NOAA High-Resolution Doppler Lidar (C. J. Grund et al. 2001, Wulfmeyer & Janjić,) measured the radial velocity of the air toward or away from the scanner. Vertical velocities in the subcloud boundary layer in DYNAMO were sampled by pointing vertically for 10 min every 20 min, alternated with constant elevation-angle azimuthal scans.

We estimate the turbulent kinetic energy (TKE) dissipation rate ϵ (Kolmogorov, 1941) in 10-min windows above 250 m (Figures 1c and 2c) from spectra of the inertial cascade of isotropic turbulence (Kaimal, 1973). Below 250 m, we estimate ϵ from transverse structure functions of the radial velocity from azimuthal scans (Figure 2c; Frehlich et al., 2006). Further details of the observations, lidar scan strategy, and ϵ calculations are summarized in supplement S1. Examples of the horizontal velocity structures at night and in the afternoon are shown in supplement S2.

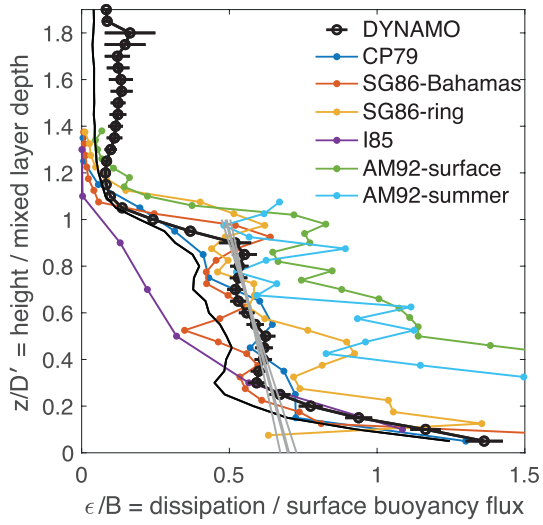

Figure 3. Turbulent kinetic energy (TKE) dissipation rate ϵ/B scaled by surface buoyancy flux in the marine atmospheric mixed layer (black circles and error bars: mean and standard deviation of the mean; thin black line: median) for Dynamics of the Madden Julian Oscillation (DYNAMO) convective conditions on Nov 13–16 and for previous estimates for terrestrial atmospheric convective boundary layers (Caughey & Palmer, 1979, blue), subsurface oceanic convective surface boundary layers (Shay and Gregg 1986: red and yellow, Anis & Moum, 1992: green and cyan), and a lake convective boundary layer (Imberger 1985, purple). Gray lines show the best fit relationship fitted on $0.4 \le z/D' \le 0.9$.

Mixed layer depth D: Most profiles in Figures 1c and 2c show turbulent MLs with $\epsilon \approx 10^{-4}$ m^2 s^{-3} below a quiescent layer with much weaker turbulence $\epsilon < 10^{-5}$ m^2 s^{-3}. We define the ML depth D as the lowest height at which ϵ is a factor of three smaller than the vertical mean ϵ below that height. ML depths were diagnosed for 2,008 profiles of ϵ in this manner (black dots Figure 2c).

Convective mixed layers: Buoyancy flux dominates the generation of TKE in DYNAMO, as in most marine atmospheric MLs. The shear production of TKE is less than the buoyancy integral ${w_*}^3 = [B]D$, where $[B]$ is the mixed-layer mean buoyancy flux. The ratio of TKE generation by surface buoyancy flux $B(0)D$ to that by shear production ${u_*}^3/\kappa$ in the ML is equal to the ratio $-D/L$ of the ML depth D to the (negative) Monin-Obukhov length $-L = {u_*}^3/\kappa B(0)$. Figure 2d shows $-D/L$ for November 13–16.

We define those MLs as convective that meet the threshold $-D/L>100$. One-third (658) of the MLs diagnosed in DYNAMO are convective according to this condition. The ratio $-D/L$ is strongly dependent on the surface wind speed. Most of the convective MLs have surface wind speed less than 2 m s^{-1}. The ratio $-D/L$ decreases approximately as wind speed U^{-3} in the shear-driven regime, and as U^{-2} in the convective regime (not shown), consistent with wind stress proportional to U^2 and buoyancy flux proportional to U (as in bulk aerodynamic models, e.g. Liu et al., 1979; Fairall et al., 1996).

The four diurnal cycles of November 13–16: Now we focus on November 13–16, when the atmospheric MLs were particularly convective. Figure 2 shows the wind and solar radiation, SST and buoyancy flux, and profiles of ϵ, and ML depth D for the 4 days. Each of the days had dSST > 1.8°C. The convective condition $-D/L>100$ (Figure 2d) was met for 96% (239) of the 249 profiles. The time-height series of ϵ for November 13–16 shows ϵ increases each afternoon (Figure 2c) over warm SST and enhanced surface buoyancy flux (Figure 2d). The ML depth D for convective ($-D/L>100$) profiles is noisy yet correlated ($R = 0.3$) with the surface buoyancy flux $B(0)$ with a sensitivity $dD/d[B(0)] = 60$ m/10^{-4} m^2 s^{-3}.

2.4. Buoyancy Flux Scaling of TKE Dissipation Rate ϵ

For the convective profiles on November 13–16, we scale each ϵ estimate by the surface buoyancy flux B, and average the profiles of ϵ/B as a function of the normalized height z/D', where $D' = 0.95D$. This scaled coordinate centers the composite mixed-layer top on the gradient of ϵ. The convective (defined by $-D/L> 100$) composite mean profile of ϵ/B is shown by black circles in Figure 3.

a) Vertical structure of the convective TKE dissipation rate profile

Close to the surface, for $z/D' \le 0.25$, ϵ/B decreases exponentially with height as $\epsilon/B = E_0 \exp\{-z/(D'H)\}$, with a surface ϵ/B of $E_0 = 1.45 \pm 0.06$ and a nondimensional scale height of $H = 0.23 \pm 0.01$. The mean ϵ/B decreases by a factor of about e^{-1} over the observed depth of the surface layer. Mechanical generation of turbulence by shear in this shallow surface layer increases ϵ/B. Mechanical generation and buoyancy flux are correlated because they mutually depend on wind speed. Nondimensional TKE dissipation rate ϵ/B as a function of $-z/L$ (not shown) is nearly uniform over $-z/L>50$ and increases in the surface layer, in agreement with aircraft measurements of marine surface layers and the universal function for ϵ/B (Fairall et al., 1980).

The DYNAMO composite ϵ/B profile is nearly uniform above the surface layer. Within $0.4 \le z/D' \le 0.9$, the mean ϵ/B and its standard error is 0.58 ± 0.02. The relative error (ratio of the standard deviation to the mean) of individual ϵ/B estimates is 0.7–0.8. The standard error of the mean ϵ/B shown in Figure 3 is divided by square root of the number of realizations. The composite ϵ/B decreases slightly with height, with

Table 1
Normalized Turbulent Kinetic Energy (TKE) Dissipation Rate Over Surface Buoyancy Flux ϵ/B Vertically Averaged Over Scaled Height $0.4 \le z/D' \le 0.9$ (± Standard Errors of the Vertical Mean) in Convective Mixed Layers (MLs) in Lakes, Oceans, and the Atmosphere

Reference	Description	Mean	Median
Imberger 1985	Lake	0.22 ± 0.06	0.22
Shay and Greg 1986	Bahamas ocean	0.47 ± 0.02	0.46
Caughey and Palmer 1979	terrestrial atmosphere	0.53 ± 0.05	0.57
Dynamics of the Madden Julian Oscillation (DYNAMO)	**marine atmosphere**	**0.58 ± 0.02**	**0.56**
Shay and Greg 1986	Gulf Stream ring	0.63 ± 0.05	0.58
Anis and Moum 1992	summer ocean	0.83 ± 0.07	0.86
Anis and Moum 1992	surface ocean	1.00 ± 0.08	1.01
grand mean		0.61 ± 0.09	0.61
grand median		0.58	0.57

a linear least squares fit of $\epsilon/B = 0.58 - (0.28 \pm 0.05)\,(z/D' - 0.65)$ (gray lines, Figure 3) passing through the middle at $z/D' = 0.65$.

The mean profile of scaled TKE dissipation rate ϵ/B for the DYNAMO marine diurnal ML agrees with the mean profiles of previously observed atmospheric, oceanic, and lacustrine convective boundary layers (Anis & Moum, 1992; Caughey & Palmer, 1979; Imberger 1985; Luce et al., 2020; Shay & Gregg 1986). DYNAMO mean ϵ/B over $0.4 \le z/D' \le 0.9$ falls in the middle of the previous estimates (Table 1), statistically indistinguishable from observations of terrestrial atmospheric (Caughey & Palmer, 1979) and Gulf Stream Ring oceanic (Shay & Gregg 1986) convective MLs.

The composite mean ϵ above the convective ML is $0.1B$ for our tropical marine atmosphere, larger than the previous studies (Figure 3). Moist convection driven by release of latent heat of condensation in clouds is responsible for intermittent turbulence above the ML. The distribution of ϵ is positively skewed (skewness of $\log\epsilon$ is 1–2), indicating infrequent strong events affect the mean. The median ϵ/B (0.05) agrees better with previous observations for $1.0 \le z/D' \le 1.4$.

2.5. Discussion of the Mixed Layer TKE Dissipation Rate Profile

Our mean $\epsilon/B = 0.58$ in the upper part of the convective ML is larger than $\epsilon/B = 0.4$ predicted by the universal function for dissipation (observed for marine layers, e.g. by Lenschow et al., 1970). The median of our ϵ/B distribution is 0.4, suggesting that convective MLs matching the universal function are common within the turbulence measurements, but that ϵ is larger in the mean. In addition to the studies compared in Figure 3, convective cold air outbreaks over the Atlantic Ocean (Chou et al., 1986) and terrestrial convection (Luce et al., 2020, Figure 9) had $\epsilon \approx 0.6B$ in the upper half of the ML.

There are several reasons the mean ϵ could be larger than the prediction for these convective MLs. Universal functions for ϵ (compiled by Kooijmans & Hartogensis 2016) are based on the convective parameter space $0 < -z/L < 5$, but MLs in our study satisfy $40 < -z/L$. The universal functions apply to an entraining ML, in which ϵ equals the vertical mean buoyancy production $0.4B(0)$ of a linear profile $B(z) = B(0)(1 - 1.2z/D)$. Free entrainment with $B(D) = 0$ applies to the observed continuous transition to moist adiabatic stratification, in which case buoyancy production-dissipation balance gives $\epsilon/B = 0.5$.

The universal function for ϵ assumes only surface shear and buoyancy flux produce TKE. Larger mean ϵ/B suggests episodic additional turbulence is generated aloft. Condensation in the intermittently cloudy moist adiabatic layer generates buoyancy flux. Cold evaporative downdrafts inject positive buoyancy flux and TKE into the ML, and cloud TKE can be transported into the ML. Figure 2c shows intermittent elevated layers of turbulence above D. Shear production linked to surface stress is negligible in the upper convective ML, yet

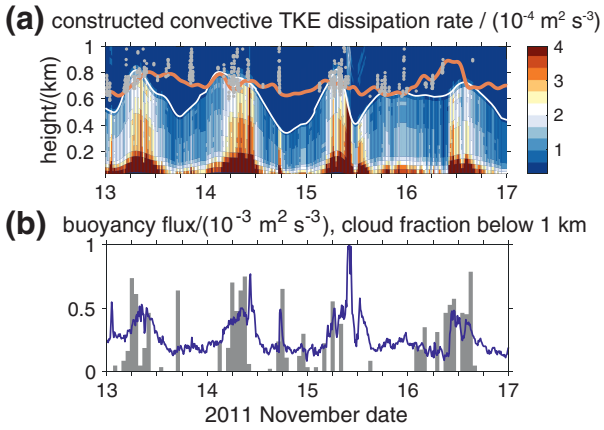

Figure 4. (a) Turbulent kinetic energy (TKE) dissipation rate reconstructed from the time series of buoyancy flux, diurnal mixed layer height, and the profile of ϵ/B for 2011 Nov 13-16. Mixed layer depth (white) and lifted condensation level (LCL, orange) of surface air temperature and humidity, filtered thrice with a 180-min moving window. Gray dots show the height of cloud bases from the ceilometer. (b) Buoyancy flux (blue) and ceilometer cloud fraction below 1 km altitude (gray bars).

elevated shear production away from the surface may generate TKE not predicted by the surface-based universal functions.

3. Connection of Diurnal Boundary Layer Convection to Clouds

The reconstructed convective ϵ is calculated by multiplying the normalized ϵ/B profile (Figure 3) by the time series of surface buoyancy flux $B(0)$ for 2011 November 13–16 UTC (Figure 4a). The buoyancy flux, and hence the idealized convective ϵ in the ML, increases by a factor of 2.7 in the afternoon compared to at night.

Mixed layer depth is also deeper during the afternoon. Figure 4a shows D filtered thrice by a 180-min running mean. The afternoon maxima of D Nov 13–16 correspond to maxima in buoyancy flux (Figure 4b) and convective ϵ (Figure 4a). When this deeper D reaches the LCL (also filtered, orange line Figure 4a), water vapor can condense and form a cloud at near the ML top (gray dots, Figure 4a; gray bars, Figure 4b, show cloud fraction below 1 km).

The ML depth falls below the LCL each evening after sunset. The LCL also lowers gradually at night due to lower temperature and higher relative humidity. The LCL reaches a minimum around dawn (about 0 UTC). The surface air dewpoint depression $T-T_d$ predicts LCL as $z_{LCL} = 40$ m+(128 m/°C)$(T-T_d)$.

4. Summary

Diurnal convective MLs over the ocean are like those over land but with weaker temperature and buoyancy flux anomalies. Weak wind simultaneously makes for weak shear and strong diurnal ocean surface temperature anomalies. The 4-day composite mean ϵ profile of diurnal convective MLs is 0.58 ± 0.02 times the surface buoyancy flux in the upper ML, scaling with surface buoyancy flux like previous observations of convective MLs in the atmosphere and oceans.

Diurnal convective turbulence generates clouds. ML depth is greatest during the afternoon when the SST is warmest and the mixed-layer ϵ is strongest. The ML depth reaches the lifting condensation level, where water vapor condenses and forms clouds. The measurements of the diurnal cycle of ϵ and D determine the turbulent fluxes into shallow clouds over the parts of the ocean experiencing weak wind, such as during phases of suppressed tropical convective precipitation.

DYNAMO had 24% of days with dSST > 1°C, more than most previous estimates. The fraction of days with dSST greater than 1°C varies widely among observational analyses. Higher-resolution satellite and in-situ measurements have higher dSST than reanalyzes (Bellenger & Duvel 2009; Clayson & Weitlich 2007). Extreme dSST from satellites exceeds 5°C (Clayson & Bogdanoff, 2013; Gentemann et al. 2003). Buoy observations from five tropical sites show dSST exceeds 1°C for 5% of days (Prytherch et al., 2013). This fraction of the oceans equatorward of 30° latitude would represent 2% of Earth's surface area.

Data Availability

The TKE dissipation rate data are available from NOAA Chemical SciencesDivision:https://esrl.noaa.gov/csl/groups/csl3/measurements/dynamo/calendar.php.

Acknowledgment
The authors gratefully acknowledge J. Moum, L. Kantha, and the anonymous reviewer for discussions that improved this manuscript. This work was supported by the NOAA OAR Climate Program Office awards NA11OAR4310076 and NA19OAR4310375, Office of Naval Research awards N00014-10-1-0299 and N00014-16-1-3094, and National Science Foundation award 1619903.

References

Anis, A., & Moum, J. N. (1992). The superadiabatic surface layer of the ocean during convection. *Journal of Physical Oceanography*, *22*(10), 1221–1227. https://doi.org/10.1175/1520-0485(1992)022<1221:TSSLOT>2.0.CO;2

Bellenger, H., & Duvel, J.-P. (2009). An analysis of tropical ocean diurnal warm layers. *Journal of Climate*, *22*(13), 3629–3646. https://doi.org/10.1175/2008JCLI2598.1

Bellenger, H., Takayabu, Y. N., Ushiyama, T., & Yoneyama, K. (2010). Role of diurnal warm layers in the diurnal cycle of convection over the tropical Indian Ocean during MISMO. *Monthly Weather Review*, *138*(6), 2426–2433. https://doi.org/10.1175/2010MWR3249.1

Caughey, S. J., & Palmer, S. G. (1979). Some aspects of turbulence structure through the depth of the convective boundary layer. *Quarterly Journal of the Royal Meteorological Society*, *105*(446), 811–827. https://doi.org/10.1002/qj.49710544606

Chen, S. S., & Houze, R. A. (1997). Diurnal variation and life-cycle of deep convective systems over the tropical pacific warm pool. *Quarterly Journal of the Royal Meteorological Society*, *123*(538), 357–388. https://doi.org/10.1002/qj.49712353806

Clayson, C. A., & Bogdanoff, A. S. (2013). *The Effect of diurnal sea surface temperature warming on climatological air–sea fluxes*. https://doi.org/10.1175/JCLI-D-12-00062.1

Clayson, C. A., & Weitlich, D. (2007). Variability of tropical diurnal sea surface temperature. *Journal of Climate*, *20*(2), 334–352. https://doi.org/10.1175/JCLI3999.1

Dai, A., & Trenberth, K. E. (2004). The diurnal cycle and its depiction in the community climate system model. *Journal of Climate*, *17*(5), 930–951. https://doi.org/10.1175/1520-0442(2004)017<0930:TDCAID>2.0.CO;2

de Szoeke, S. P., Edson, J. B., Marion, J. R., Fairall, C. W., & Bariteau, L. (2015). The MJO and air-sea interaction in TOGA COARE and DYNAMO. *Journal of Climate*, *28*(2), 597–622. https://doi.org/10.1175/JCLI-D-14-00477.1

Eastman, R., & Warren, S. G. (2014). Diurnal Cycles of cumulus, cumulonimbus, stratus, stratocumulus, and fog from surface observations over land and ocean. *Journal of Climate*, *27*(6), 2386–2404. https://doi.org/10.1175/JCLI-D-13-00352.1

Fairall, C. W., Bradley, E. F., Rogers, D. P., Edson, J. B., & Young, G. S. (1996). Bulk parameterization of air-sea fluxes for Tropical Ocean-Global Atmosphere Coupled-Ocean Atmosphere Response Experiment. *Journal of Geophysical Research*, *101*(C2), 3747–3764.

Fairall, C. W., Markson, R., Schacher, G. E., & Davidson, K. L. (1980). An aircraft study of turbulence dissipation rate and temperature structure function in the unstable marine atmospheric boundary layer. *Boundary-Layer Meteorology*, *19*(4), 453–469. https://doi.org/10.1007/BF00122345

Frehlich, R., Meillier, Y., Jensen, M. L., Balsley, B., & Sharman, R. (2006). Measurements of boundary layer profiles in an urban environment. *Journal of Applied Meteorology and Climatology*, *45*(6), 821–837. https://doi.org/10.1175/JAM2368.1

Frisch, A. S., & Ochs, G. R. (1975). A note on the behavior of the temperature structure parameter in a convective layer capped by a marine inversion. *Journal of Applied Meteorology*, *14*(3), 415–419. https://doi.org/10.1175/1520-0450(1975)014<0415:ANOTBO>2.0.CO;2

Gentemann, C. L., & Akella, S. (2018). Evaluation of NASA GEOS-ADAS modeled diurnal warming through comparisons to SEVIRI and AMSR2 SST observations. *Journal of Geophysical Research: Oceans*, *123*(2), 1364–1375. https://doi.org/10.1002/2017JC013186

Gentemann, C. L., Donlon, C. J., Stuart-Menteth, A., & Wentz, F. J. (2003). Diurnal signals in satellite sea surface temperature measurements. *Geophysical Research Letters*, *30*(3), 1140. https://doi.org/10.1029/2002GL016291

Gray, W. M., & Jacobson, R. W. (1977). Diurnal variation of deep cumulus convection. *Monthly Weather Review*, *105*(9), 1171–1188. https://doi.org/10.1175/1520-0493(1977)105<1171:DVODCC>2.0.CO;2

Grund, C. J., Banta, R. M., George, J. L., Howell, J. N., Post, M. J., Richter, R. A., & Weickmann, A. M. (2001). High-resolution doppler lidar for boundary layer and cloud research. *Journal of Atmospheric and Oceanic Technology*, *18*(3), 376–393. https://doi.org/10.1175/1520-0426(2001)018<0376:HRDLFB>2.0.CO;2

Grund, C. J., Banta, R. M., George, J. L., Howell, J. N., Post, M. J., Richter, R. A., & Weickmann, A. M. (2001a). High-resolution doppler lidar for boundary layer and cloud research. *Journal of Atmospheric and Oceanic Technology*, *18*(3), 376–393. https://doi.org/10.1175/1520-0426(2001)018<0376:HRDLFB>2.0.CO;2

Hughes, K. G., Moum, J. N., & Shroyer, E. L., 2020: Heat transport through diurnal warm layers. *Journal of Physical Oceanography*, *50*, 2885–2905. https://doi.org/10.1175/JPO-D-20-0079.1

Imberger, J. (1985). The diurnal mixed layer. *Limnology & Oceanography*, *30*(4), 737–770. https://doi.org/10.4319/lo.1985.30.4.0737

Kaimal, J. C. (1973). Turbulence spectra, length scales and structure parameters in the stable surface layer. *Boundary-Layer Meteorology*, *4*(1), 289–309. https://doi.org/10.1007/BF02265239

Kaimal, J. C., Wyngaard, J. C., Haugen, D. A., Coté, O. R., Izumi, Y., Caughey, S. J., & Readings, C. J. (1976). Turbulence structure in the convective boundary layer. *Journal of the Atmospheric Sciences*, *33*(11), 2152–2169. https://doi.org/10.1175/1520-0469(1976)033<2152:TSITCB>2.0.CO;2

Kawai, Y., & Wada, A. (2007). Diurnal sea surface temperature variation and its impact on the atmosphere and ocean: A review. *Journal of Oceanography*, *63*(5), 721–744. https://doi.org/10.1007/s10872-007-0063-0

Kolmogorov, A. N. (1941). Dissipation of energy in locally isotropic turbulence (Vol. 32, pp. 16–18). *Presented at the dokl. Akad. Nauk SSSR*.

Kooijmans, L. M. J., & Hartogensis, O. K. (2016). Surface-layer similarity functions for dissipation rate and structure parameters of temperature and humidity based on eleven field experiments. *Boundary-Layer Meteorology*, *160*(3), 501–527. https://doi.org/10.1007/s10546-016-0152-y

LeMone, M. A., & Pennell, W. T. (1976). The relationship of trade wind cumulus distribution to subcloud layer fluxes and structure. *Monthly Weather Review*, *104*(5), 524–539. https://doi.org/10.1175/1520-0493(1976)104<0524:TROTWC>2.0.CO;2

Lenschow, D. H. (1970). Airplane measurements of planetary boundary layer structure. *Journal of Applied Meteorology*, *9*(6), 874–884. https://doi.org/10.1175/1520-0450(1970)009<0874:AMOPBL>2.0.CO;2

Liu, W. T., Katsaros, K. B., & Businger, J. A. (1979). Bulk Parameterization of air-sea exchanges of heat and water-vapor including the molecular constraints at the interface. *Journal of the Atmospheric Sciences*, *36*(9), 1722–1735.

Luce, H., Kantha, L., Hashiguchi, H., Doddi, A., Lawrence, D., & Yabuki, M. (2020). On the relationship between the TKE dissipation rate and the temperature structure function parameter in the convective boundary layer. *Journal of the Atmospheric Sciences*, *77*(7), 2311–2326. https://doi.org/10.1175/JAS-D-19-0274.1

Madden, R. A., & Julian, P. R. (1971). Detection of a 40-50 day oscillation in the zonal wind in the tropical Pacific. *Journal of the Atmospheric Sciences*, *28*(5), 702–708.

Matthews, A. J., Baranowski, D. B., Heywood, K. J., Flatau, P. J., & Schmidtko, S. (2014). The surface diurnal warm layer in the Indian Ocean during CINDY/DYNAMO. *Journal of Climate*, *27*(24), 9101–9122. https://doi.org/10.1175/JCLI-D-14-00222.1

Moulin, A. J., Moum, J. N., & Shroyer, E. L. (2017). Evolution of turbulence in the diurnal warm layer. *Journal of Physical Oceanography*, *48*(2), 383–396. https://doi.org/10.1175/JPO-D-17-0170.1

Moum, J. N., de Szoeke, S. P., Smyth, W. D., Edson, J. B., DeWitt, H. L., Moulin, A. J., et al. (2014). Air–sea interactions from westerly wind bursts during the November 2011 MJO in the Indian Ocean. *Bulletin of the American Meteorological Society*, *95*(8), 1185–1199. https://doi.org/10.1175/BAMS-D-12-00225.1

Price, J. F., Weller, R. A., & Pinkel, R. (1986). Diurnal cycling: Observations and models of the upper ocean response to diurnal heating, cooling, and wind mixing. *Journal of Geophysical Research*, *91*, (C7), 8411. http://dx.doi.org/10.1029/jc091ic07p08411

Prytherch, J., Farrar, J. T., & Weller, R. A. (2013). Moored surface buoy observations of the diurnal warm layer. *Journal of Geophysical Research: Oceans*, *118*(9), 4553–4569. https://doi.org/10.1002/jgrc.20360

Randall, D. A., Harshvardhan, & Dazlich, D. A. (1991). Diurnal variability of the hydrologic cycle in a general circulation model. *Journal of the Atmospheric Sciences*, *48*(1), 40–62. https://doi.org/10.1175/1520-0469(1991)048<0040:DVOTHC>2.0.CO;2

Ruppert, J. H., & Johnson, R. H. (2016). On the cumulus diurnal cycle over the tropical warm pool. *Journal of Advances in Modeling Earth Systems*. https://doi.org/10.1002/2015MS000610

Ruppert, J. H., Jr, & Johnson, R. H. (2015). Diurnally Modulated cumulus moistening in the preonset stage of the Madden–Julian oscillation during DYNAMO. *Journal of the Atmospheric Sciences*, *72*(4), 1622–1647. https://doi.org/10.1175/JAS-D-14-0218.1

Shay, T. J., & Gregg, M. C. (1986). Convectively driven turbulent mixing in the upper ocean. *Journal of Physical Oceanography*, *16*(11), 1777–1798. https://doi.org/10.1175/1520-0485(1986)016<1777:CDTMIT>2.0.CO;2

Sui, C.-H., Lau, K.-M., Takayabu, Y. N., & Short, D. A. (1997). Diurnal variations in tropical oceanic cumulus convection during TOGA COARE. *Journal of the Atmospheric Sciences*, *54*(5), 639–655. https://doi.org/10.1175/1520-0469(1997)054<0639:DVITOC>2.0.CO;2

Thompson, E. J., Moum, J. N., Fairall, C. W., & Rutledge, S. A. (2019). Wind limits on rain layers and diurnal warm layers. *Journal of Geophysical Research: Oceans*, *124*(2), 897–924. https://doi.org/10.1029/2018JC014130

Tian, B., Soden, B. J., & Wu, X. (2004). Diurnal cycle of convection, clouds, and water vapor in the tropical upper troposphere: Satellites versus a general circulation model. *Journal of Geophysical Research: Atmosphere*, *109*(D10). https://doi.org/10.1029/2003JD004117

Yasunaga, K., Fujita, M., Ushiyama, T., Yoneyama, K., Takayabu, Y. N., & Yoshizaki, M. (2008). Diurnal variations in precipitable water observed by shipborne GPS over the tropical Indian Ocean. *Inside Solaris*, *4*, 97–100. https://doi.org/10.2151/sola.2008-025

References From the Supporting Information

Anis, A., & Moum, J. N. (1994). Prescriptions for heat flux and entrainment rates in the upper ocean during convection. *Journal of Physical Oceanography*, *24*(10), 2142–2155. https://doi.org/10.1175/1520-0485(1994)024<2142:PFHFAE>2.0.CO;2

Brown, R. A. (1970). A secondary flow model for the planetary boundary layer. *Journal of the Atmospheric Sciences*, *27*, 742–757. https://doi.org/10.1175/1520-0469(1970)027<0742:ASFMFT>2.0.CO;2

Brown, R. A. (1972). On the inflection point instability of a stratified Ekman boundary layer. *Journal of the Atmospheric Sciences*, *29*, 850–859. https://doi.org/10.1175/1520-0469(1972)029<0850:otipio>2.0.co;2

Browning, K. A., & Wexler, R. (1968). The determination of kinematic properties of a wind field using doppler radar. *Journal of Applied Meteorology*, *7*(1), 105–113. https://doi.org/10.1175/1520-0450(1968)007<0105:TDOKPO>2.0.CO;2

Ciesielski, P. E., Yu, H., Johnson, R. H., Yoneyama, K., Katsumata, M., Long, C. N., et al. (2014). Quality-controlled upper-air sounding dataset for DYNAMO/CINDY/AMIE: Development and corrections. *Journal of Atmospheric and Oceanic Technology*, *31*(4), 741–764. https://doi.org/10.1175/JTECH-D-13-00165.1

Deardorff, J. W. (1976). On the entrainment rate of a stratocumulus-topped mixed layer. *Quarterly Journal of the Royal Meteorological Society*, *102*(433), 563–582. https://doi.org/10.1002/qj.49710243306

de Szoeke, S. P., Skyllingstad, E. D., Zuidema, P., & Chandra, A. S. (2017). Cold pools and their influence on the tropical marine boundary layer. *Journal of the Atmospheric Sciences*, *74*(4), 1149–1168. https://doi.org/10.1175/JAS-D-16-0264.1

Frehlich, R., & Cornman, L. (2002). Estimating spatial velocity statistics with coherent doppler lidar. *Journal of Atmospheric and Oceanic Technology*, *19*(3), 355–366. https://doi.org/10.1175/1520-0426-19.3.355

Gregg, M. C., D'Asaro, E. A., Riley, J. J., & Kunze, E. (2018). Mixing efficiency in the ocean. *Annual Review of Marine Science*, *10*(1), 443–473. https://doi.org/10.1146/annurev-marine-121916-063643

Howard, L. (1803). *On the modification of clouds*. Retrieved from https://digital.nmla.metoffice.gov.uk/SO_0f0df589-3560-4ecf-815d-0b9285e6608a/

LeMone, M. A. (1973). The structure and dynamics of horizontal roll vortices in the planetary boundary layer. *Journal of the Atmospheric Sciences*, *30*, 1077–1091, https://doi.org/10.1175/1520-0469(1973)030<1077:TSADOH>2.0.CO;2

Lemone, M. A. (1976). Modulation of turbulence energy by longitudinal rolls in an unstable planetary boundary layer. *Journal of the Atmospheric Sciences*, *33*(7), 1308–1320. https://doi.org/10.1175/1520-0469(1976)033<1308:MOTEBL>2.0.CO;2

Lenschow, D. H., Wulfmeyer, V., & Senff, C. (2000). Measuring second- through fourth-order moments in noisy data. *Journal of Atmospheric and Oceanic Technology*, *17*(10), 1330–1347. https://doi.org/10.1175/1520-0426(2000)017<1330:MSTFOM>2.0.CO;2

Moran, K. P., Pezoa, S., Fairall, C. W., Williams, C., Ayers, T., Brewer, W. A., et al. (2012). A motion stabilized W-band radar for shipboard cloud observations and airborne studies of sea spray. *Journal of Boundary Layer Meteorology*, *143*(1), 3–24. https://doi.org/10.1007/s10546-011-9674-5

O'Connor, E. J., Illingworth, A. J., Brooks, I. M., Westbrook, C. D., Hogan, R. J., Davies, F., & Brooks, B. J. (2010). A method for estimating the turbulent kinetic energy dissipation rate from a vertically pointing doppler lidar, and independent evaluation from balloon-borne in situ measurements. *Journal of Atmospheric and Oceanic Technology*, *27*(10), 1652–1664. https://doi.org/10.1175/2010JTECHA1455.1

Pope, S. B. (2000). *Turbulent flows*. Cambridge University Press. Retrieved from https://books.google.com/books?id=HZsTw9SMx-0C

Sreenivasan, K. R. (1995). On the universality of the Kolmogorov constant. *Physics of Fluids*, *7*(11), 2778–2784. https://doi.org/10.1063/1.868656

Tucker, S. C., Brewer, W. A., Banta, R. M., Senff, C. J., Sandberg, S. P., Law, D. C., et al. (2009). Doppler lidar estimation of mixing height using turbulence, shear, and aerosol profiles. *Journal of Atmospheric and Oceanic Technology*, *26*(4), 673–688.

Winters, K. B., Lombard, P. N., Riley, J. J., & D'Asaro, E. A. (1995). Available potential energy and mixing in density-stratified fluids. *Journal of Fluid Mechanics*, *289*, 115–128. https://doi.org/10.1017/S002211209500125X

Wulfmeyer, V., & Janjić, T. (2005). Twenty-four-hour observations of the marine boundary layer using shipborne NOAA high-resolution doppler lidar. *Journal of Applied Meteorology*, *44*(11), 1723–1744. https://doi.org/10.1175/JAM2296.1